COMSOL CONFERENCE 2019 CAMBRIDGE

Flow and Heat Transfer through an Open-Cell Metal Foam

B. Chinè[1*], V. Mussi [2], A. Rossi [2]
1. School of Materials Science and Engineering, Costa Rica Institute of Technology, Cartago Costa Rica
2. Laboratorio MUSP, Macchine Utensili e Sistemi di Produzione, Piacenza, Italy
*Corresponding author: P.O. Box 159-7050, Cartago, Costa Rica, bchine@itcr.ac.cr

1. Introduction

Open-cell metal foams (or metal sponge) are interesting materials with many potential uses. These materials can be used to enhance heat transfer in many applications, such as cryogenic heat exchanger, compact heat sinks and heat exchanger, as remarked by Lu et al. [1]. They are characterized by a cellular structure represented by a metal (or a metal alloy) and connected gas voids inside (Fig. 1). Due to their intrinsic high porosity and large specific surface area [2], these materials are considered to have very promising properties to improve efficiency and minimize the required weight and volume of novel industrial heat exchangers. In that case, the complexity of the convective heat transfer process and the number of parameters to analyze simultaneously, demand a preliminary and hugely wide experimental activity to design foamed components with a good quality for energy transferring systems. The development of computational models might help to reduce experimental works and costs, although the task is very challenging. Numerical studies modelling porous media have been used to capture the details of the intricate sponge structure while considering the porous solid-fluid systems as homogeneous [3]. Moreover, computational attempts modelling representative elementary volume (REV) of a sponge with its solid and void phases have also shown encouraging results [2,3,4]. Krishnan et al. [5] studied the fluid and heat flow in a periodic unit cell and obtained effective thermal conductivity, pressure drop and local heat transfer from a consistent direct simulation of the open-cell foam structure. Interesting computational models based on X ray micro-tomographic scans of the sponge geometry have been developed by many authors, among others Meinicke et al. [6] and, recently, Dixit and Gosh [7] and Jafarizade et al. [8]. Bayomy and Saghir [9] investigated the heat transfer characteristics of aluminum foam heat sink for electronic cooling, developing three different geometries of the sink. The authors used the software Comsol Multiphysics® to evaluate and successfully compare the distributions of temperature, Nusselt numbers and pressure drops of the three sinks. On the other hand, Bidar et al. [10] developed a computational model of forced convective heat transfer to study the airflow through a two-sided vertical channel filled with open-cell metal foams with 10 ppi (pores per linear inch) and specific values of porosity. Application of the RANS equations to model the airflow inside ceramic foams used in solar heat recovery has been carried out by Wu et al. [11]. Odabaee and Hooman [12] reported numerical results on the reduction of the air-side thermal resistance from a four row heat exchanger, containing aluminium tubes wrapped by metal

Figure 1. An open-cell metal foam.

foam in cross-flow. Finally, Mancin et al. [13] have measured experimental heat transfer coefficients by means of an interesting experimental work, which considered air flow heating in different aluminum open-cell foam samples, under a wide range of air mass velocity.

In this work, we use COMSOL Multiphysics® 5.4 to model the fluid flow and heat transfer process through a three dimensional open-cell aluminium foam of a heat exchanger. In the device, the heat is transferred from a stream of hot water to a cold air flow. The study takes in consideration convection and diffusive mechanisms in the fluids and heat conduction in the solid regions of the system.

The structure of the paper is the following. The description of the physical model and the governing equations are given in Section 2, whereas Section 3 describes the use of Comsol Multiphysics®. Finally, the computational results are presented in Section 4 and the conclusions in Section 5.

2. Physical model and governing equations

Fig. 2 shows a schematic of the heat exchanger section modeled in the present study, with geometrical dimensions given also in Table 1. The length L of the section is 26 mm, its width a is 10.4 mm and the height H is equal to 8.45 mm. In the device, the cold air stream flows in a parallelepiped component made of aluminium sponge, with a rectangular cross section of height b equal to 5.2 mm and of the same width a. On the top of this section there is a channel for the hot water flow with a length in z direction equal to a and a rectangular cross section of width c (20.8 mm) and height d (2.6 mm). A very thin solid layer, made of aluminium with a thickness h of 0.65 mm, separate the two fluid streams.

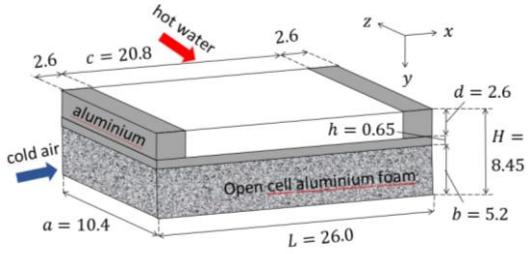

Figure 2. Geometry, main dimensions (in mm) of the heat exchanger section and x,y,z coordinate system of reference.

Table 1. Dimensions of the modeled heat exchanger section.

Magnitude	*Value*
Length L	26.00 mm
Width a	10.40 mm
Height H	8.45 mm
Height b of the aluminium sponge	5.20 mm
Width c of the water channel	20.80 mm
Height d of the water channel	2.60 mm
Height h of the thin aluminium solid layer	0.65 mm

Using the values of Table 2, it is modeled the geometry of an ideal, open-cell aluminum foam by first generating a unit cubic solid block of edge length l. Next, three mutually perpendicular cylinders of radius R and length l are placed inside the block. By subtracting the three cylinders from the cubic block, it is obtained a porous cell inscribed in the cube, surrounded by solid struts with variable edge thickness. In each cross plane cutting the block, the struts thickness is between eh and $\sqrt{2}\,(R + eh) - R$. Moreover, the length l of the cubic edge is equal to $2(R + eh)$. Next, arrays of identical unit cells are created in the space to generate the 3D open-cell metal foam, made up of uniform distributed equal sized-cubic cells. In this way, the struts separating two consecutive cells have a minimum thickness equal to $2eh$. Finally, an identical rotation of 30° with respect to each axis of the coordinate systems is applied to the previous array, thus avoiding the formation of circular channels oriented as x, y and z, respectively. We consider two aluminium sponge with different values of porosity and specific surface area (or surface area density), which are fundamental magnitudes characterizing the structure of an open-cell foam. Table 2 specifies dimensions of the cubic cell, porosity and specific surface area of the two metal sponges.

In the physical model, the weakly compressible cooling air flow through the connected voids of the sponge, and the incompressible hot water flow in the channel are both assumed as steady state and laminar and then coupled to the heat transfer mechanisms. The governing equations are the conservation of the thermal energy, represented by the Fourier equation with convective terms (Eq.1) and the mass conservation and the linear momentum conservation described by the Navier-Stokes equations (Eqs. 2 and 3). For a steady dependent process, in vector form they read

Table 2. Dimensions of two aluminium sponges.

Aluminium sponge 1	
Length l of the unit cube edge	2.60 mm
Radius R of the inner cylinders	1.20 mm
Length l of the inner cylinders	2.60 mm
Minimum thickness eh of the cell strut	0.10 mm
Minimum thickness $2eh$ of a strut between two consecutive cells	0.20 mm
Pore density	~ 10 pores per linear inch
Volume of the pores V_p	1.25721×10^{-6} m^3
Volume of the solid struts V_s	1.4889×10^{-7} m^3
Porosity $\epsilon = V_p / V_s$	89.41%
Surface area of the struts S_s	8.13×10^{-4} m^2
Total volume of the aluminium sponge V_f	1.4061×10^{-6} m^3
Specific surface area of the aluminium sponge S_s / V_f	578 m^2/ m^3
Aluminium sponge 2	
Length l of the unit cube edge	2.60 mm
Radius R of the inner cylinders	1.25 mm
Length l of the inner cylinders	2.60 mm
Minimum thickness eh of the cell strut	0.05 mm
Minimum thickness $2eh$ of a strut between two consecutive cells	0.1 mm
Pore density	~ 10 pores per linear inch
Volume of the pores V_p	1.29379×10^{-6} m^3
Volume of the solid struts V_s	1.1231×10^{-7} m^3
Porosity $\epsilon = V_p / V_s$	92.01%
Surface area of the struts S_s	6.69×10^{-4} m^2
Total volume of the aluminium sponge V_f	1.4061×10^{-6} m^3
Specific surface area of the aluminium sponge S_s / V_f	476 m^2/ m^3

$$\rho C_p \mathbf{u} \nabla T = \nabla \bullet (k \nabla T) + Q \qquad (1)$$

$$\nabla \cdot (\rho \mathbf{u}) = 0 \qquad (2)$$

$$\rho (\mathbf{u} \bullet \nabla)\mathbf{u} = \nabla \bullet [-p\mathbf{I} + \eta (\nabla \mathbf{u} + (\nabla \mathbf{u})^T) - \frac{2\eta}{3} (\nabla \bullet \mathbf{u})\mathbf{I}] + \mathbf{F} \qquad (3)$$

In Eq. 1 T is the temperature and ρ, $\mathbf{u}$, k, C_p and Q are the fluid density, fluid velocity, thermal conductivity, specific heat capacity at constant pressure and heat source, respectively. Moreover, in Eqs. 2 and 3 η is the dynamic viscosity and p is the pressure, whereas $\mathbf{I}$ and $\mathbf{F}$ represent the identity tensor and body forces, respectively.

We apply appropriate boundary conditions to the thermal energy equation, by assuming for the heat exchanger section: a) at the inlets, temperature $T_{in,\,a}$ of 300 K for the air inflow and temperature $T_{in,\,w}$ of 330 K for the water inflow; b) at the outlets, $-\mathbf{n} \bullet \mathbf{q} = 0$ for both fluids, where $\mathbf{q}$ is the heat flux and $\mathbf{n}$ is the normal direction; c) conditions of symmetry on the bottom of the heat exchanger section; d) conditions of thermal insulation on the rest of the surfaces. Instead, for the computation of the velocity field we set: a) at the inlet, a normal velocity $U_{in,w}$ of 0.05 m/s for the water flow and three different values (0.5 m/s, 1 m/s and 1.5 m/s) for the normal velocity $U_{in,a}$ of the cooling air; b) at the outlets, a null gauge pressure; c) conditions of symmetry on the top of the water channel and the bottom of the air flow; d) conditions of open boundary (normal stresses equal to zero) on the side walls of the foam section, simulating a contact with a large volume of fluid; e) boundary condition of no slip on the rest of the solid surfaces, including the solid walls of the open-cell foam.

3. Solution with Comsol Multiphysics®

We study the steady state fluid flow and heat transfer process through the three dimensional heat exchanger section by using the Heat Transfer [14] and CFD [15] modules of Comsol Multiphysics® 5.4. To couple the two mechanisms we select the Conjugate Heat Transfer physics interface. In the model, heat is transferred from a laminar stream of hot water to a laminar flow of cold air by convection and diffusive phenomena in the fluids and by conduction in the solid regions of the system, i.e., walls of device and metal sponge. We assume the solid as aluminium alloy Al 6063-T83 with density of 2700 kg/m^3, thermal conductivity of 201 W/(m·K) and heat capacity at

constant pressure of 900 J/(kg·K). Using the capabilities of the Geometry Node, we start our modelling work by generating the geometry of the open-cell metal foam (as described previously) and the exchanger section.

To preserve the flow structure in the upstream and downstream of the heat exchanger, the computational domain is extended of 20 mm in the *x* direction, by extruding of 10 mm the cross section of both air inlet and outlet, obtaining a total length of 46 mm. A detailed description on the importance of enveloping the model geometry is reviewed in [6]. Boundary conditions of no slip for the fluid flow and thermal insulation for the heat transfer are set on the wall of these new surfaces. However, the flow entering the heat exchanger section is still not fully developed, because the computed hydrodynamic entry length is much greater than 10 mm, even for the simulated smallest velocity of 0.5 m/s. The values of inlet cross sectional area A_{cs}, wetted perimeter of the flow channel L_p, hydraulic diameter D_h, temperature at inlet T_{in}, thermosphysical properties, inlet velocity U, mass flow rate $\dot{m}$, Reynolds number Re_h, hydrodynamic entry length $x_{fd,h}$ and thermal entry length $x_{fd,t}$ are given in Table 3 for the air and water inflows, using the data of Incropera et. al [16]. At the least, the rest of boundary conditions are specified in order to solve the resulting system of partial differential equations of the model (Eqs. 1, 2 and 3).

Next, we apply an unstructured meshing of the computational region accomplished by dividing it with free tetrahedral volumes and using *fine* element in the computational region, with maximum element size of $4.97\text{x}10^{-4}$ mm and minimum element size of $9.37\text{x}10^{-5}$ mm. Additionally, boundary layers are created on the solid walls, using default values of the software. Finally, the number of degrees of freedom (DFOs) to be solved for is approximately $8.5\text{x}10^{6}$ plus $5\text{x}10^{5}$ internal DOFs for all the simulated cases.

4. Results and discussion

In the following, the computational results are displayed for the aluminium sponge 2 with a porosity of 92.01% and setting at the air cooling inlet a velocity $U_{in,a}$ of 1.5 m/s. The other parameters are constant, i.e, water velocity $U_{in,w}$ of 0.05 m/s, water temperature $T_{in,w}$ of 330 K and

Table 3. Experimental values used to study the conjugated heat and fluid flow:

a) Air inflow at 300 K with 3 different inlet velocities

Magnitude	*Value*
Inlet cross sectional area $A_{cs} = (a \text{ x } b)$	$5.408\text{x}10^{-5}$ m^2
Wetted perimeter of the flow channel $L_p=2\ (a + b)$	$3.120\text{x}10^{-2}$ m
Hydraulic diameter $D_h = 4A_{cs} / L_p$	$6.933\text{x}10^{-3}$ m
Temperature at inlet $T_{in,a}$	300 K
Density ρ (at 1atm)	1.1614 kg/m^3
Dynamic viscosity μ (at 1atm)	$1.846\text{x}10^{-5}$ Pa·s
Heat capacity at constant pressure c_p (at 1atm)	1.007 kJ/(kg·K)
Prandtl number Pr (at 1atm)	0.707
Inlet velocity $U_{in,a}$	0.5 m/s 1 m/s 1.5 m/s
Mass flow rate $\dot{m} = \rho U_{in,a} A_{cs}$	$3.140\text{x}10^{-5}$ kg/s $6.281\text{x}10^{-5}$ kg/s $9.421\text{x}10^{-5}$ kg/s
Reynolds number $Re_h = \rho\ U_{in,w}\ D_h / \mu$	218 436 654
Hydrodynamic entry length $x_{fd,h} \approx 0.05\ Re_h\ D_h$	75.6 mm 151.2 mm 226.8 mm
Thermal entry length $x_{fd,t} \approx 0.05\ Re_h\ D_h\ Pr$	53.5 mm 106.9 mm 160.3 mm

b) Water inflow at 330 K with a constant inlet velocity

Magnitude	*Value*
Inlet cross sectional area $A_{cs} = (c \text{ x } d)$	$5.408\text{x}10^{-5}$ m^2
Wetted perimeter of the flow channel $L_p=2\ (c + d)$	$4.680\text{x}10^{-2}$ m
Hydraulic diameter $D_h = 4A_{cs} / L_p$	$4.622\text{x}10^{-3}$ m
Temperature at inlet $T_{in,w}$	330 K
Density ρ (at p_{sat})	984 kg/m^3
Dynamic viscosity μ (at p_{sat})	$0.489\text{x}10^{-3}$ Pa·s
Heat capacity at constant pressure c_p (at p_{sat})	4.184 kJ/(kg·K)
Prandtl number Pr (at p_{sat})	3.15
Inlet velocity $U_{in,w}$	0.05 m/s
Mass flow rate $\dot{m} = \rho U_{in,w} A_{cs}$	$0.266\text{x}10^{-2}$ kg/s
Reynolds number $Re_h = \rho U_{in,w} D_h / \mu$	465
Hydrodynamic entry length $x_{fd,h} \approx 0.05\ Re_h\ D_h$	107.5 mm
Thermal entry length $x_{fd,t} \approx 0.05\ Re_h\ D_h\ Pr$	338.5 mm

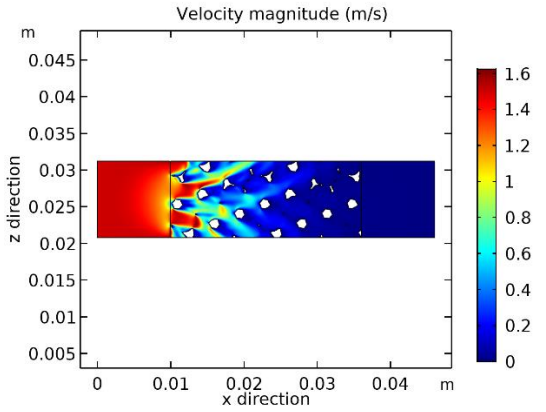

Figure 3. Air velocity magnitude (m/s) in the middle of the heat exchanger section ($U_{in,a}$ = 1.5 m/s, θ = 92.01%).

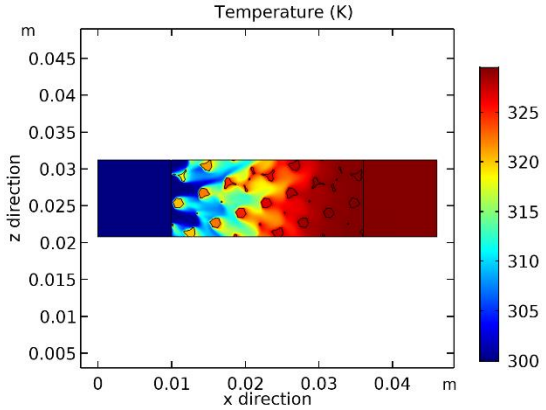

Figure 4. Air temperature (K) in the middle of the heat exchanger section ($U_{in,a}$ = 1.5 m/s, θ = 92.01%).

cooling air temperature $T_{in,a}$ of 300 K. Figs. 3 and 4 show, respectively, air velocity magnitude and temperature on a horizontal *xz* surface placed in the middle (y=0.026 m) of the heat exchanger section. Instead, Fig. 5 and 6 depict a vertical view (*xy* plane) of the velocity magnitude and temperature, respectively. These results highlight that the temperature of the cooling air increases continuously as it flows along the heat exchanger section, due to tortuous paths promoting local mixing of fluid, and thereby directly causing an increase in the local heat transfer rate. The computational results of the conjugate flow and heat transfer confirm the strong coupling between velocity and temperature fields, showing the effect of the solid ligaments (heat conduction) on the solution of the thermal energy conservation of the surrounding air. As plotted in Figs. 3 and 5, the velocity of the cooling air is decreasing due to the presence of the open-cell metal foam, which slows down the convective flow of the air when crossing the intricate structure of this material. Figs. 4 and 6 shows that, along the heat exchanger section, the temperature of the cooling air is approaching that of the water, taking advantage of the material's high porosity and large specific surface area. A temperature profile in the direction of air flow (Fig. 7) illustrates the pattern, being evident that large temperature fluctuations exist longitudinally, manifestation of the presence of either void (pore) or the metallic struts. Dixit and Gosh [7] have given similar results also. In Figs. 8 and 9, two temperature profiles in the y vertical direction (on the central longitudinal *xz* plane) are plotted for a region close to the air inlet (x=0.0135 m) and air outlet (x=0.0328 m), respectively. The results show as the temperature

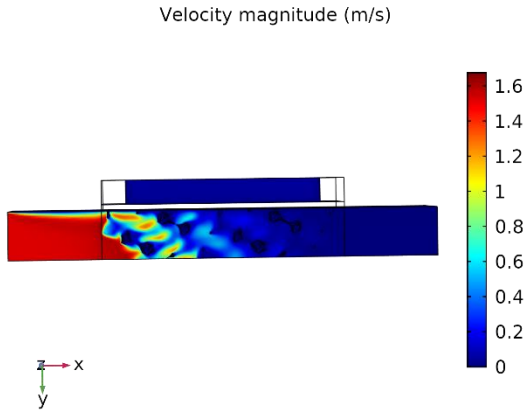

Figure 5. Vertical view of the air velocity pattern in the heat exchanger section ($U_{in,a}$ = 1.5 m/s, θ = 92.01%).

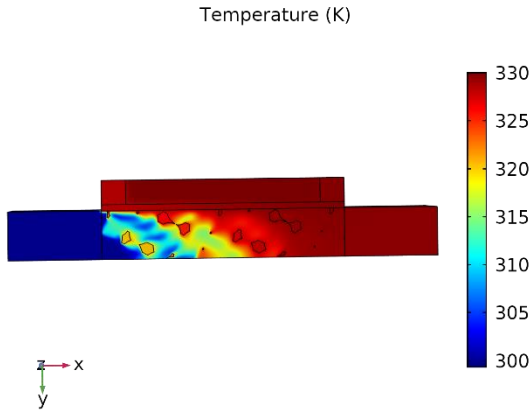

Figure 6. Vertical view of the temperature pattern in the heat exchanger section ($U_{in,a}$ = 1.5 m/s, θ = 92.01%).

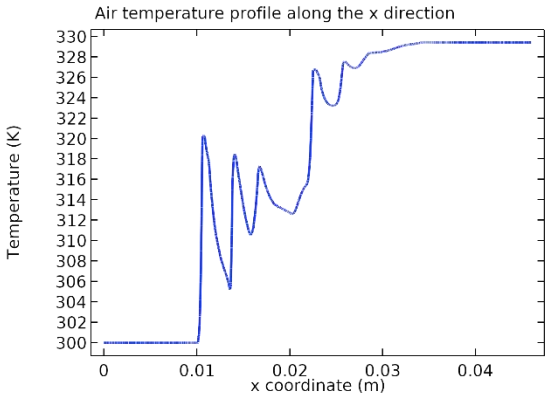

Figure 7. Air temperature profile in the direction of air flow, in the middle of the heat exchanger section (y= 0.026 m, z= 0.026 m, $U_{in,a}$ = 1.5 m/s, θ = 92.01%).

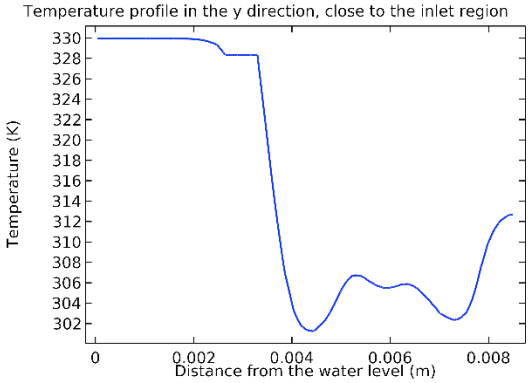

Figure 8. Air temperature profile in the y direction close to the inlet region (x= 0.0135 m), on the central longitudinal plane (z= 0.026 m) of the heat exchanger section ($U_{in,a}$ = 1.5 m/s, θ = 92.01%).

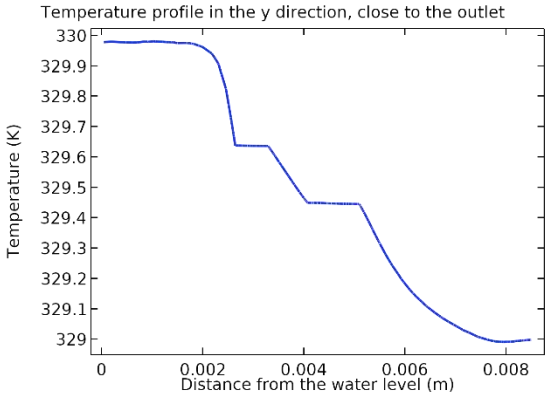

Figure 9. Air temperature profile in the y direction close to the outlet region (x= 0.0328 m), on the central longitudinal plane (z= 0.026 m) of the heat exchanger section ($U_{in,a}$ = 1.5 m/s, θ = 92.01%).

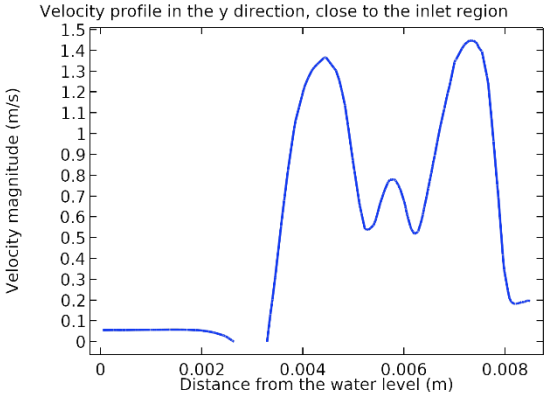

Figure 10. Air velocity profile in the y direction close to the inlet region (x= 0.0135 m), on the central longitudinal plane (z= 0.026 m) of the heat exchanger section ($U_{in,a}$ = 1.5 m/s, θ = 92.01%).

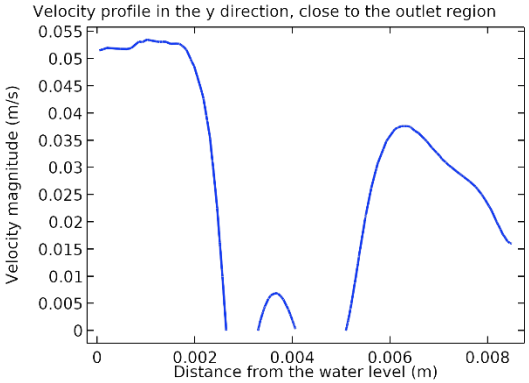

Figure 11. Air velocity profile in the y direction close to the outlet region (x= 0.0328 m), on the central longitudinal plane (z= 0.026 m) of the heat exchanger section ($U_{in,a}$ = 1.5 m/s, θ = 92.01%).

varies transversally and maintains fluctuations in proximity of the solid foam struts. The plot of Fig. 9 remarks that, near the outflow of the simulated heat exchanger section, the air temperature is approaching the water temperature. Finally, the corresponding velocity profiles are given in Figs. 10 and 11 for the same regions of the device. The computational results underline the peculiar structure of the air velocity, with values varying in the transverse direction to the flow, due to the fluid moving between solid ligaments of the connected pores.

5. Conclusions

The numerical findings of the simulations show that the computational model developed

with COMSOL Multiphysics® is effective for modelling the conjugate flow and heat transfer process through a 3D open-cell aluminium foam. Furthermore, the results prove that the energy transfer of the exchanger highly depends on the flow structure, taking advantage of the material's high porosity and large specific surface area. The computational model is able to capture the main properties of the coupled heat and fluid flow and can be considered a valid approach to evaluate open-cell metal foams' performance for heat transfer applications. According to these results, we foresee to carry out developments of the modeling work by using CAD of real open-cell foams and evaluating the efficiency of heat exchangers in terms of pressure drop and transferred energy.

6. References

[1] T.J. Lu, H.A. Stone and M.F. Ashby, Heat transfer in open-cell metal foams, *Acta Materialia*, **46**(10), 3619-3635, (1998).

[2] K. Boomsma, D. Poulikakos and F. Zwick, Metal foams as compact high performance heat exchangers, *Mechanics of Materials*, **35**, 1161-1176, (2003).

[3] A. Kopanidis, A. Theodorakakos, E. Gavaises and D. Bouris, 3D Numerical simulation of flow and conjugate heat transfer through a pore scale model of high porosity open cell foam, *Int. Journ. of Heat and Mass Transfer*, **53**, 2539-2550, (2010).

[4] K. Boomsma, D. Poulikakos and Y. Ventikos, Simulation of flow through open cell metal foams using an idealized periodic cell structure, *Int. Journ. of Heat and Fluid Flow*, **24**, 825-834, (2003).

[5] S. Krishnan, J.Y. Murthy and S.V. Garimella, Direct simulation of transport in open-cell metal foam, *ASME Journ. of Heat Transfer*, **128**, 793-799, (2006).

[6] S. Meinicke, T. Wetzel and B. Dietrich, CFD Modeling of single-phase hydrodynamics and heat transfer in solid sponges, *11th Int. Confer. on CFD in the Minerals and Process Industry-CSIRO*, Melbourne, Australia, 7-9 December (2015).

[7] T. Dixit and I. Ghosh, Simulation intricacies of open-cell metal foam fin subjected to convective flow, *App. Thermal Engin.*,**137**, 532-544, (2018).

[8] A. Jafarizade, M. Panjepour, M. Meratian and M.D. Emami, Numerical simulation of gas/solid heat transfer in metallic foams: A general correlation for different porosities and pore sizes, *Transport in porous media*, **122**(3), DOI 10.1007/s11242-018-1208-x, (2018).

[9] A.M Bayomy. and M.Z. Saghir, Experimental and numerical study of aluminium metal foam (with/without channels) subjected to steady water flow, *Pertanika Journal of Science and Technology*, **25**(1), 221-246 (2017).

[10] B. Bidar, F. Shahraki and D. M. Kalhori, 3D Numerical modelling of convective heat transfer through two-sided vertical channel symmetrically filled with metal foams, *Periodica Polytechnica Mech. Engineer*., **60**(4), 193-2012, (2016).

[11] Z. Wu, C. Caliot, G. Flamant and Z. Wang, Numerical simulation of convective heat transfer between air flow and ceramic foams to optimise volumetric solar air receiver performances, *Int. Journ. of Heat and Mass Transfer*, **54**, 1527-1537, (2011).

[12] M. Odabaee and K. Hooman, Metal foam heat exchangers for heat transfer augmentation from a tube bank, *App. Thermal Engin.*, **36**, 456-463, (2012).

[13] S. Mancin, C. Zilio, A. Cavallini and L. Rossetto, Heat transfer during air flow in aluminum foams, *Int. Journ. of Heat and Mass Transfer*, **53**, 4976-4984, (2010).

[14] Comsol AB, Comsol Multiphysics-Heat Transfer Module, *User's Guide*, Version 5.4 (2018).

[15] Comsol AB, Comsol Multiphysics-CFD Module, *User's Guide*, Version 5.4 (2018).

[16] F. P. Incropera et al., *Fundamentals of heat and mass transfer*, John Wiley and Sons, Hoboken (NJ), USA (2007).

7. Acknowledgements

The authors gratefully acknowledge the financial aid provided by the Vicerrectoria de Investigaciòn y Extensiòn of the Instituto Tecnològico de Costa Rica through the project 1351022.